Full length article

Robocasting of Cu²⁺ & La³⁺ doped sol–gel glass scaffolds with greatly enhanced mechanical properties: Compressive strength up to 14 MPa

Basam A.E. Ben–Arfa, Sofia Neto, Isabel M. Miranda Salvado *, Robert C. Pullar *, José M.F. Ferreira

Department of Materials and Ceramic Engineering/CICECO – Aveiro Institute of Materials, University of Aveiro, 3810–193 Aveiro, Portugal

ARTICLE INFO

ABSTRACT

This research details the successful fabrication of scaffolds by robocasting from high silica sol–gel glass doped with Cu^{2+} or La^{3+}. The parent HSSGG composition within the system SiO_2–CaO–Na_2O–P_2O_5 [67% Si – 24% Ca – 5% Na – 4% P (mol%)] was doped with 5 wt% Cu^{2+} or La^{3+} (Cu5 and La5). The paper sheds light on the importance of copper and lanthanum in improving the mechanical properties of the 3–D printed scaffolds. 1 h wet milling was sufficient to obtain a bioglass powder ready to be used in the preparation of a 40 vol% solid loading paste suitable for printing. Moreover, Cu addition showed a small reduction in the mean particle size, while La exhibited a greater reduction, compared with the parent glass. Scaffolds with macroporosity between 300 and 500 μm were successfully printed by robocasting, and then sintered at 800 °C. A small improvement in the compressive strength (7–18%) over the parent glass accompanied the addition of La. However, a much greater improvement in the compressive strength was observed with Cu addition, up to 221% greater than the parent glass, with compressive strength values of up to $\sim$14 MPa. This enhancement in compressive strength, around the upper limit registered for human cancellous bones, supports the potential use of this material in biomedical applications.

Statement of Significance

3D porous bioactive glass scaffolds with greatly improved compressive strength were fabricated by robocasting from a high silica sol–gel glasses doped with Cu^{2+} or La^{3+}. In comparison to the parent glass, the mechanical performance of scaffolds was greatly improved by copper-doping (>220%), while a modest increase of $\sim$9% was registered for lanthanum-doping. Doping ions (particularly La^{3+}) acted as glass modifiers leading to less extents of silica polymerisation. This favoured the milling of the glass powders and the obtaining of smaller mean particle sizes. Pastes with a high solid loading (40 vol%) and with suitable rheological properties for robocasting were prepared from all glass powders. Scaffolds with dimensions of 3 × 3 × 4 mm and macro-pore sizes between 300 and 500 μm were fabricated.

1. Introduction

Bioactive glasses demonstrate high degrees of rapid response to body fluids and encourage new cell growth, both *in–vitro* and *in–vivo*. However, they also typically have weak mechanical properties [1]. There exist many functional ions that although existing in trace quantities in human body play important different roles and are vital for a good body metabolism. Doping a bioactive glass with some of these functional ions in trace quantities has also been shown to improve their properties [2,3]

Copper (Cu) is found throughout the tissues of the human body in total trace quantities of $\sim$75–100 mg. Of this quantity, 50% of the Cu is stored in the muscles and bones [4]. Cu is also a vital component in gene–expression [5], and since it serves as a cofactor [6], Cu aids about 30 enzymes to provide the proper function [7]. Cu works as an antioxidant preventing free radicals from damaging the walls of cells. Moreover, Cu is an essential element for keeping blood vessels, connective tissues and skin in a healthy condition [7]. Cu deficiency may lead to inappropriate bone formation, as well as fracture of the bones, particularly in children. In patients with bone fractures, it is found that Cu–supplements reduce the healing time [8]. Much work has been carried out on doping Cu in bioactive glasses and composites for biomedical applications. For example, in a composite of poly methyl methacrylate (PMMA) and

* Corresponding authors.
E-mail addresses: isabelmsalvado@ua.pt (I.M. Miranda Salvado), rpullar@ua.pt (R.C. Pullar).

Cu–doped glass, the system showed good bioactivity, and antibacterial action towards staphylococcus epidermidis [2] and Escherichia coli [9]. Borate glass doped with copper showed promising results in healing full–thickness skin wounds [10]. It was also found that the inclusion of Cu in bioactive glass increases vascularisation and augments bone formation [11]. Bioactive glasses doped with 2–5 mol% Cu have shown good bioactivity and antimicrobial properties against E. coli, S. aureus and S. epidermidis bacteria, with a better overall *in vitro* performance being observed for 2 mol% Cu [12]. This Cu doping level was within the 0.1–2.5 wt% range reported to enhance the *in vitro* performance of bioactive glass [13]. Moreover, a composite of mesoporous glass with 5 mol% Cu (MBG-5Cu) was reported to considerably improve angiogenesis compared with the control [14]. Wu et al. [15] prepared bioactive glass scaffolds doped with 0–5 mol% Cu which exhibited enhanced angiogenesis properties, drug loading and release capability, and antibacterial properties. Furthermore, the specific surface area and pore volume tended to decrease with increasing Cu content from 0 to 5 mol% [15]. This is a good attribute for powders used in the preparation of ink for printing scaffolds by robocasting.

Lanthanum (La) is a rare earth element, which has no biological role in humans, and its bioavailability in the human body is extremely low, at 0.00127% (±0.00080%) [16]. Commonly La does not exist in the animal and plants tissue; nevertheless, it is found in traces in drinking water [17], and in elevated quantities (up to 16 times higher than non-exposed controls) with amounts (∼0.5 $\mu g\ g^{-1}$) in bones and lungs of refinery and smelter workers [18]. Despite this, it has a wide range of applications in treatments to repair disorders in the human body, such as playing an important role in treating atherosclerotic cardiovascular disease when taken as a lanthanum chloride supplement [19]. Furthermore, if taken as supplement in the form of lanthanum carbonate it can partially replace the calcium–based phosphate which occurs in hypercalcemia, leading to cardiovascular calcification [17], or the case of hyperphosphatemia in patients with end stage renal disease (ESRD) [20].

Adding trace amounts of La to 45S5 glass (up to 0.5 wt%) resulted in improved bioactivity, while beyond this value La retarded the bioactivity of bioglass[®] [21]. There is much evidence to suggest that lanthanum tends to deposit in bone, and addition of La^{3+} ions demonstrated a pronounced enhancement of *in–vitro* osteoblast differentiation [22]. Treatment of titanium surfaces with La, implanted in both rats and rabbits, led to increases in protein adsorption, resulting in an improved healing response of the bone [23], and in hydroxyapatite (HAp)–La composites, better mechanical properties were observed than when using pure HAp in bone implants [24].

The bioactivity of the high silica sol–gel glass (HSSGG) in a powder form [25], the bioactivity and biocompatibility of a scaffold using HSSGG [26], and the bioactivity and biocompatibility of Cu and La doped glasses [27] were recently investigated and addressed by the authors. Therefore, it is interesting to look at the effects of these two additives on sol–gel derived bioglasses, and fabricated glass or glass–ceramic scaffolds. Literature review reveals that no Cu and/or La doped glasses have been used so far as precursors to produce 3–D scaffolds by robocasting. Sol–gel derived glasses have many advantages (lower sintering temperatures, more intimate mixing of components, greater porosity), but the inherent porosity of sol–gel derived glass powders causes problems during preparation of robocasting pastes, as their high level of porosity can adsorb liquid from the pastes affecting viscosity and flow behaviour during printing. The authors have addressed the problem previously in a Ca–Si–P–Na based 4 component sol–gel glass system [28].

A scaffold is a 3–D structure constructed to be a temporary implant, acting as a template for new cell growth, and which degrades during/after the healing process, while the seeded cells grow and proliferate to regenerate new tissue [29]. Scaffolds need to meet particular morphological requirements: they need to have large interconnected pores and a hierarchical degree of porosity, requiring macro–pore sizes > 50 μm to enable cells to easily penetrate the scaffold structure, and micro pore sizes < 50 μm to facilitate cell anchorage and proliferation. The macrospores play an important role for tissue regeneration [30], as ∼100 μm pores may introduce a hypoxia environment (deprived of adequate oxygen) which leads to osteochondral formation before osteogenesis [31]. At a larger pore size of ∼150, it was observed that osteons began to form [32]. Scaffolds with several pore sizes from 106 to 600 μm were fabricated from hydroxyapatite and implanted in rats for *in vivo* assessments. A higher rate of bone formation was observed in the scaffolds with a pore size in the range of 300–400 [31]. Other research groups observed dominant bone ingrowth at an optimised pore size of 450 μm for a scaffold produced from poly(methyl methacrylate) (PMMA) [33]. Moreover, it was demonstrated that for nerve system regeneration, for instance, the long-size peripheral axons required a pore size of ∼700 μm or larger [34]. Scaffolds must also exhibit moderate mechanical strength to resist any applied loads, while avoiding the effect of stress shielding that can result in bone loss [35,36]. A large degree of macro–sized interconnectivity is also a crucial element, to enable cells to migrate into to the centre of the scaffold, and to allow a sufficient supply of nutrients for cell growth [36].

Robocasting offers a better control of the macro–pore shape and size, as well as the possibility to produce customised implants for an individual patient. The robotic control of the ink deposition also enables the assembling of specific predesigned complex shapes and morphologies to replace the defect part of a bone in a very precise manner, using CAD–CAM technology [37].

Very little work has been carried out regarding the robocasting of bioactive glass fabricated by melt–quenching method for 3–D scaffolds [38,39], while the use of sol–gel glass is still a new field for robocasting, the authors being pioneers in this area. To the authors' knowledge, there have been no previous investigations into the use of doped sol–gel bioactive glass as precursors to fabricate 3–D scaffolds by robocasting. This work is devoted to improving the mechanical properties, with copper or lanthanum additives, of quaternary–system, high–silica content bioactive sol–gel derived glass scaffolds made by robocasting.

2. Materials and methods

2.1. Sol–gel glass synthesis

A four–component high silica sol–gel bioactive glass in the SiO_2–CaO–Na_2O–P_2O_5 system with a composition [67% Si – 24% Ca – 5% Na – 4% P (mol%)], hereafter labelled HSSGG, was synthesised by employing a rapid sol–gel route, as described previously by the authors [25].

Tetra–ethyl–ortho–silicate (TEOS, $C_8H_{20}O_4Si$, 98%), triethyl phosphate (TEP, $C_6H_{15}O_4P$, ≥99.8%), calcium nitrate tetrahydrate (CaN, $Ca(NO_3)_2·4H_2O$, ≥99%), sodium nitrate (NaN, $NaNO_3$, ≥99%), Copper(II) nitrate trihydrate (CuN, $Cu(NO_3)_2·3H_2O$, ≥99%), and Lanthanum(III) nitrate hexahydrate (LaN, $La(NO_3)_3·6H_2O$, ≥99.9%) were used as precursors. All six precursors were supplied from Sigma–Aldrich. Distilled water was used as solvent and citric acid monohydrate (CA, $C_6H_8O_7·H_2O$, 99.5–102%, Sigma–Aldrich) was added to catalyse the sol–gel hydration and polymerisation reactions.

The two doped glasses containing 5 wt% each of either La^{3+} or Cu^{2+} ions were prepared based on the parent (HSSGG) glass. The Cu or La precursors were added to the homogeneous sols obtained according to the procedures described previously by the authors [25] to study their separate influence on the scaffold printing ability, and on the corresponding mechanical properties of the sintered scaffolds. The doped glass compositions are hereafter designated as Cu5 and La5. The batch compositions (in both wt% and mol%) are presented in Table 1.

2.2. Wet milling procedure

The acquired gels were dried by means of rotary evaporator (Buchi 210 Rotavapor with V–850 vacuum controller and V–700 diaphragm vacuum pump), in a 500 mL pear–shaped flask while rotating in a water bath at 55 °C and under a low pressure of 50 mbar for 30 min. The as–dried gels were heat treated up to 800 °C using the following regime: From room temperature to 200 °C with heating rate of 1 °C min^{-1} and soaking time of 30 min; followed by increasing the temperature to 400 °C with a heating rate of 2 °C min^{-1} and soaking time of 30 min; and from 400 to 800 °C with heating rate of 5 °C, and soaking time of 2 h, to be followed by natural cooling to room temperature.

The heat treated powders were pulverised using wet ball milling. Ethanol (EtOH) served as a milling medium, EtOH to powder mass ratio (EPR) = 1.5, balls to powder mass ratio (BPR) = 10, and 1 h milling time. The milling was performed in a S–series–Fast Mill machine, type S2–1000 (Ceramic Instruments, Sassuolo, Italy), with a rotational speed of 390 rpm, using 300 cm^3 capacity alumina jar (Ceramic instruments Sassuolo, Italy). 10 mm diameter Yttria–stabilised zirconia balls (Tosoh, Tokyo, Japan), were used as milling medium. After milling, the obtained slurry was separated for drying in an oven at 60 °C for 24 h. The dry powders were passed through a 63 μm sieve to separate the large agglomerates from the fine powder. The fine powder was characterised using the following techniques:

2.3. Characterisation of the milled powder

Particle size (PS) and the particle size volume distribution (PSD) were investigated using a laser diffraction particle size analyser (Coulter LS particle size analyser; Beckman Coulter, CA). Measurements were triplicated to guarantee accurate results.

The effects of ion doping on the polymerisation silica networks were assessed by magic angle spinning–magnetic nuclear resonance (MAS–NMR) for ^{29}Si NMR environment. X-ray diffraction (XRD) was used to follow–up the evolution of the crystalline phases upon doping. The XRD patterns) were acquired using a PANalytical XPERT–PRO Diffractometer system with Cu–Kα radiation (Kα = 1.540 Å), with 2Θ varying from 6 to 70° in steps of 0.026 s^{-1}, and the diffraction patterns were compared with JCPDS standards. Density determination for the scaffolds was performed using the buoyancy (Archimedes') method by immersing the samples in distilled water. The bulk density of the glass pellets was calculated via the following relation [40]:

$$\rho_b = \frac{m_1}{m_3 - m_2} \cdot \rho_w \qquad (1)$$

where: ρ_b is the bulk density in (g cm^{-3}); ρ_w is the density of the water, assumed to be 1 g cm^{-3}; m_1 is the mass of the dry sintered pellet measured in air; m_2 is the mass of the sintered pellet suspended in water; m_3 is the mass of the water saturated pellet measured in air.

2.4. Suspension preparation

To study the effects of the dopants on the rheological properties and printability of the inks, suspensions were prepared from the three glass powders at a solid loading fraction of (40 vol%). The powder was dispersed in de–ionised water in the presence of 1.1 wt% carboxymethyl cellulose (CMC) (Mw = 250,000, Lamberti Iberia s.a.u., Castellón, Spain). CMC serves as a multipurpose processing additive (dispersant, binder and gelation agent) [41]. The powder was added in small dosages, followed by mixing in a planetary centrifugal mixer (ARE–250, Thinky Corp. Tokyo, Japan) to assure a homogeneous suspension.

2.5. Rheological characterisation of suspensions and pastes

The rheological properties of the suspensions were evaluated using a Kinexus Pro + Rheometer (Malvern Instruments). The viscometry mode was used to measure the apparent viscosity of the tested samples, using the cone (4°/40 mm) and plate sensor system with a 150 μm gap size. The viscoelastic properties of the pastes were measured using the oscillatory mode of the rheometer equipped with plate & plate sensor (20 mm), with 1 mm gap size. In all rheological measurements, a metal ring with deionised water as solvent trap was used to prevent water evaporation from the samples while testing.

2.6. Fabrication of scaffolds by robocasting

The bioactive glass scaffolds were deposited layer–by–layer using robocasting equipment (3–D Inks, Stillwater, OK). The paste was extruded through a 410 μm diameter nozzle using a printing speed of 10 mm s^{-1}. The designed scaffold was constructed from 12 deposited layers, each layer consisting of 5 parallel rods, and with the next layer perpendicular to the plane of the rods. The porous structures were printed in assemblies containing nine scaffolds, with three different pore sizes (the distance between the rods) of 300, 400 and 500 μm, all with dimensions of (3x3x4) mm. The deposition was carried out in a reservoir containing paraffin oil to allow a uniform drying of the green scaffolds. After printing completion, the scaffolds were removed from the oil and dried at room temperature for 24 h, followed by sintering at 800 °C for 2 h, using a heating rate of 1 °C min^{-1} for the entire heating cycle, to ensure a complete removal of residual organics.

2.7. Compressive strength evaluation

The compressive strength of sintered scaffolds was determined under uniaxial tests using 10 samples of each pore size series (300,

Table 1
Batch compositions of all synthesised glasses in mol%, and wt%

Glass	Si		Na		Ca		P		Cu		La	
	wt%	mol%	wt%	mol%	wt%	mol%	wt%	mol%	wt%	Mol%	wt%	Mol%
HSSGG	67.0	64.4	5	5	24.0	21.5	4.0	9.1	0	0	0	0
Cu5	64.3	61.2	4.8	4.7	23.0	20.5	3.8	8.6	4	5	0	0
La5	66.3	61.2	5	4.7	23.7	20.5	4	8.64	0.00	0.00	1	5

400, and 500 μm). The tests were carried on a universal testing machine (AG–IS10kN, Shimadzu, Kyoto, Japan) at a constant speed of 0.5 mm min^{-1} in the perpendicular direction to the printing plane.

2.8. Statistical analysis

The porosity and compressive strength results will be expressed as the mean value ± standard deviation (SD) from six measurements.

A population of six samples (n = 6) were used to compare the acquired data from compressive strength tests. A two way analysis of variance (two-way ANOVA) tests was performed for three samples (HSSGG, La5, and Cu5) with three different macropore sizes (300, 400 and 500 μm), assuming following null hypothesis:

H$_1$ = the means of observations grouped by the different glass samples (1st factor) are the same.

H$_2$ = the means of observations grouped by the different macroporosities (2nd factor) of the scaffold are the same.

H$_3$ = No interaction between the two factors.

Moreover, one-way ANOVA was used to express clearly the significant difference and improvement in the compressive strength between HSSGG, La5, and Cu5 glasses for each individual macropore size of 300, 400 and 500 μm. The null and alternative hypotheses for one-way ANOVA are:

H$_0$ = the means of observations grouped by the different macroporosities of the scaffold made from same material are equal.

H$_1$ = all the means are not equal. The alpha level is considered to be (α = 0.05).

The null hypothesis will be rejected if ANOVA Fisher value (F) is greater than the critical value (F > F$_{crit}$), and the P-value is smaller than the alpha value (P < 0.05). This shows that significant differences exist between all the means of compressive strength.

3. Results and discussion

3.1. The effects of ion doping on particle size distribution

Fig. 1(a, b and c) show particle sizes distributions for HSSGG, Cu5 and La5 glasses, respectively. The effects of each individual doping ion on PSD were evaluated. As can be observed from Fig. 1, all PSDs exhibit 3–modal profiles. HSSGG shows larger particle sizes (Fig. 1(**a**)) than the two doped glasses. A decrease in the particle size was observed for Cu5 (Fig. 1(**b**)), and a further decrease in particle size was observed in La5 (Fig. 1(**c**)). Moreover, the area of the 3rd fitted peak in PSD, representing the coarser fraction, is getting gradually smaller and the modal sizes gradually shift from ∼19 μm in HSSGG to ∼14 μm (Cu5), and then to ∼11 μm (La5). The ionic radius of Cu (0.73 Å) is much smaller than that of La (1.06 Å) [42]. The difference in ionic radii of metal (M) cations is likely to affect the average coordination number with oxygen atoms and the M−O bond length and strength, even in an amorphous structure that is more compliant than a crystalline one. This is to say that the possible role of ionic radius on the ease of particle size reduction cannot be discarded, although data shedding light on this issue could not be found in the available literature. However, both Cu and La are well-known to act as glass modifiers leading to less polymerised silica–networks. This is confirmed by the ^{29}Si NMR spectra of the three glasses displayed in Fig. 2. The parent glass (HSSGG) exhibits the highest degree of network polymerisation. The Cu5 glass shows a somewhat less polymerised structure, while a more extensive disruption in the silica–network is observed for the La5 glass. Experimental evidences about the network modifier role of La$_2$O$_3$ in silicate glasses were recently
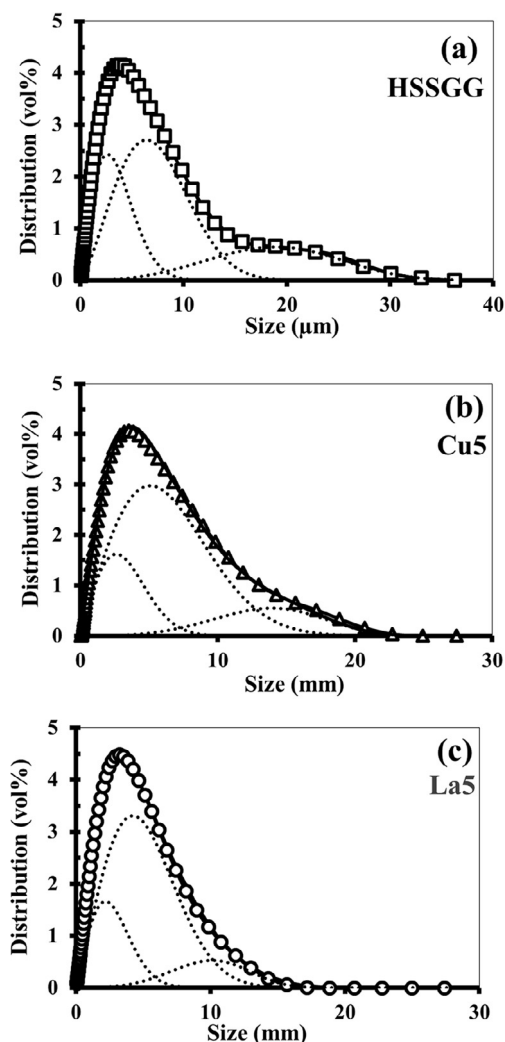

Fig. 1. The ion doping effects on the particles size distributions of the wet-milled glass powders: (a) HSSGG, (b) Cu5 and (c) La5.
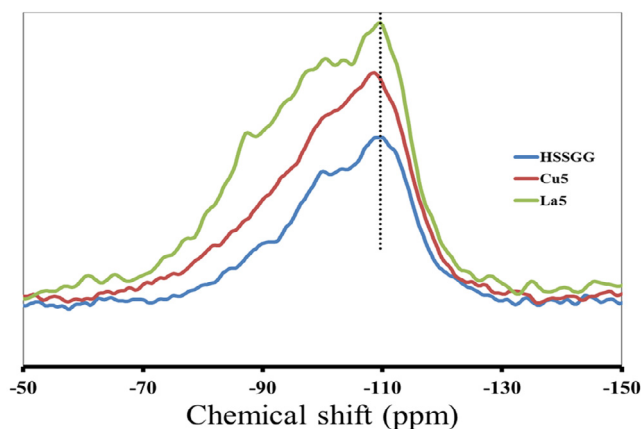

Fig. 2. ^{29}Si NMR for HSSGG (blue line), Cu5 (brown line) and La (green line) doped glasses. (For interpretation of the references to colour in this figure legend, the reader is referred to the web version of this article.)

reported [43]. All these results support the hypothesis that the less polymerised networks of doped glasses facilitate breakage of the particles into smaller sizes.

3.2. The effects of ion doping on crystalline phase evolution

X-ray diffraction patterns of parent and La- and Cu-doped glasses are displayed in Fig. 3. A completely amorphous material was obtained upon submitting the HSSGG to a heat treatment temperature (HTT) up to 700 °C [28]. The results presented in Fig. 3 show that further increasing the HTT to 800 °C leads to partial crystallisation. The following three crystalline phases could be identified: cristobalite (SiO$_2$; pdf # 04–007–2134), wollastonite (CaSiO$_3$, pdf # 04–011–2265), and hydroxyapatite (Ca$_5$(PO$_4$)$_3$(OH), pdf # 04-013 − 6615). Cristobalite is the major crystalline phase formed in HSSGG, followed by wollastonite. The intensity of the XRD peaks of these crystalline phases was enhanced for doped glasses, with particularly an increased intensity of hydroxyapatite peaks in the case of Cu5 glass.

3.3. Rheological characterisation of suspensions and pastes

3.3.1. Apparent viscosity

The apparent viscosity curves *versus* shear rate for the suspensions prepared from HSSGG, Cu5 and La5 powders are presented in Fig. 4. In all cases, the apparent viscosity decreases with the increase in shear rate in a similar manner. This shear thinning behaviour is an essential prerequisite for ink extrusion through fine nozzles. Within the range of low shear rate, the high apparent viscosity values measured can be assigned to the role played by the entangled CMC species, which led to a significant increase in the intrinsic viscosity of the suspension. As a result of increasing the shear rate, the CMC species are likely to align in the flow direction and the internal structure will gradually break down decreasing the apparent viscosity. In the region 0.1–10 s^{-1}. HSSGG exhibits the highest apparent viscosity level followed by Cu5 and La5, respectively. However, in the region from 10 to 100 s^{-1}, HSSGG maintains the same behaviour, while Cu5 and La5 show a slight increase in comparison. The sequence of flow curves in terms of apparent viscosity levels within the region from 10 to 100 s^{-1} coincides with the order of the three glass powders in terms of average particle size and broadness of PSD. This suggests that the differences observed in apparent viscosity are likely due to the physical features of the starting powders. The internal network structure promoted by the CMC species is likely less disturbed at lower shear rates when the particles are coarser, since larger interstices are left among them in comparison to a finer powder. At the higher shear rates, where hydrodynamic interactions prevail over the intermolecular ones, all three different suspensions behave more similarly, with a continuous reduction of apparent viscosity.
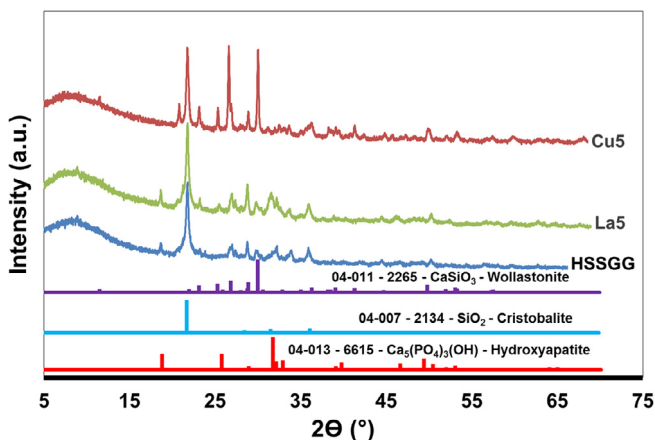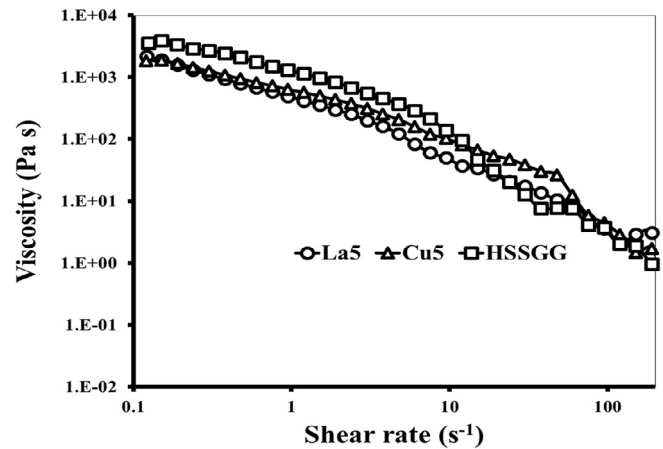
Fig. 4. Comparison of the flow properties of suspensions prepared from HSSGG, Cu5 and La5 glass powders.

3.3.2. Viscoelastic properties

Fig. 5 displays the elastic modulus (G') of the three glass inks as a function of complex shear stress. It can be seen that the measured G' values are sufficiently high for printing (Ǵ ~1×10^5 – 1×10^6 Pa) for all three glass pastes with a solid loading of 40 vol%. Interestingly, the order of the G' curves is the same observed for apparent viscosity curves plotted in Fig. 4. Cu–doping caused a small drop in G', and La–doping caused a further and more accentuated drop in the stiffness of the paste. Moreover, all pastes exhibit a continuous linear viscoelastic region (LVR) that extends nearly to 100 Pa for the HSSGG system, becoming gradually narrower for the Cu5 and La5 pastes. These results support the hypothesis discussed above that internal network structure promoted by the CMC species is likely less disturbed under low deformations as those prevailing within the LVR.

Broad LVR coupled with the high values of Ǵ are the main features required for ink printability [37,41]. This means that the dissolved and entangled CMC species, together with 40 vol% solid loading, confer to the paste the stiffness and the viscoelastic properties essential for extrusion and shape preservation of the filaments during the robocasting process. Therefore, these pastes are eminently suitable for robocasting. This is confirmed by the good shape retention observed in the SEM micrographs of sintered scaffolds presented in Fig. 6(**a–d**). The general overviews Fig. 6(**a & b**) reveal that the successive layers were successfully printed without

Fig. 3. Comparison of the XRD patterns of parent HSSGG composition with La5 and Cu5-containing samples.

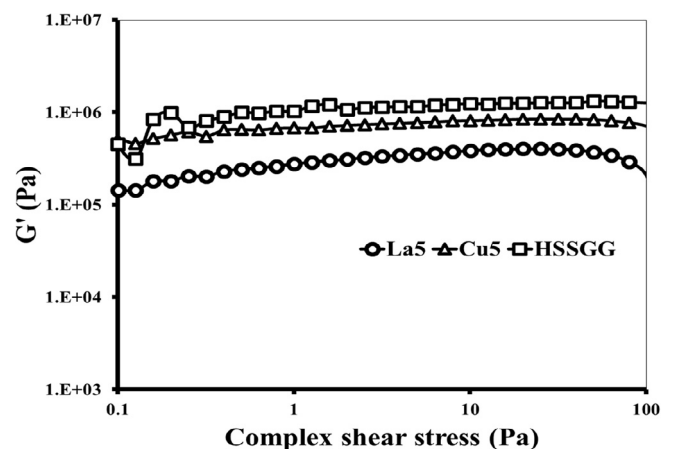**Fig. 5.** Elastic modulus (Ǵ) and extent of LVR as a function of complex shear stress of suspensions/pastes prepared from HSSGG, Cu5 and La5 glass powders.
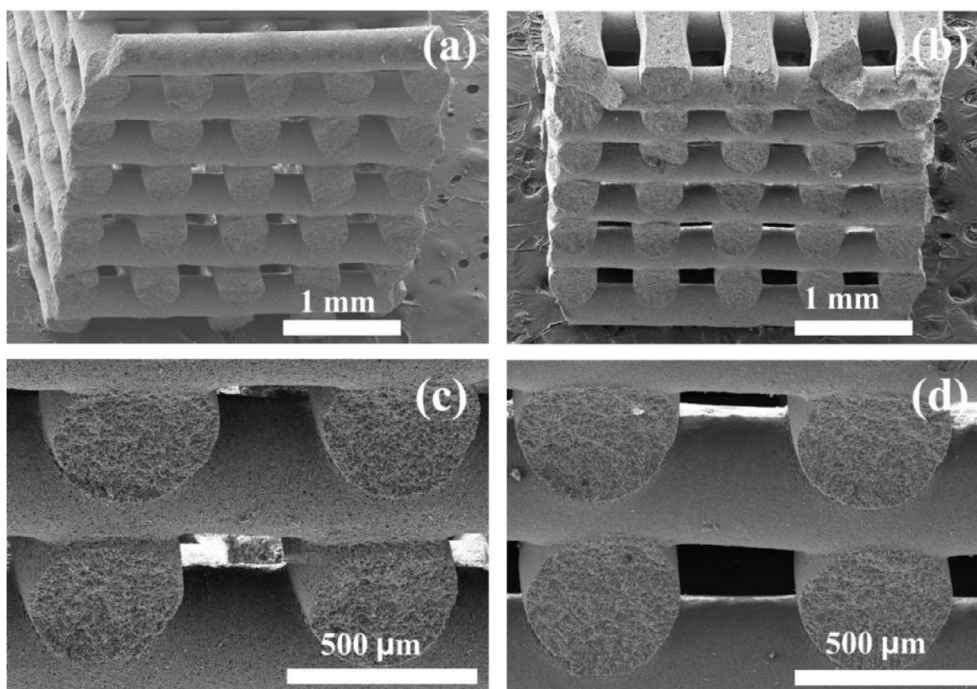
Fig. 6. Scaffolds printed from pastes of ion doped glasses: (a, c) Cu5; (b, d) La5.

disturbing the layers beneath, and the detailed views, Fig. 6(**c & b**) show that good densification levels have been achieved.

3.4. Compressive strength

All compressive strength values measured for the sintered scaffolds with the three pore sizes (300, 400 and 500 μm) are reported in Table 2. Fig. 7 also displays the values and trends. A predictable decrease in the compressive strength values with incremental pore sizes from 300 to 500 μm is observed for all the glass compositions. The compressive strength for HSSGG scaffolds varied between the limits of 2.20 ± 0.12–4.96 ± 15 MPa, which are within the range reported for human cancellous (trabecular) bone (2–12 MPa) [44], with the lowest and the highest values being registered for the largest (500 μm) and smallest (300 μm) pore sizes, respectively. A slight improvement in mechanical properties was registered for La5, where the compressive strength value was between the limits of 2.60 ± 0.35 MPa (500 μm) and 5.41 ± 30 MPa (300 μm). This means increases between 7% and 18% over that measured for HSSGG. However, great and impressive improvements in mechanical properties were observed for the Cu5 glass, with compressive strength values varying between 4.97 ± 0.28 MPa (500 μm) and 13.96 ± 0.28 MPa (300 μm), which are 125%–221% greater than those obtained for HSSGG. The value of ∼14 MPa exceeds the highest reported values for cancellous bone. The greatest increase of 221% in compressive strength over HSSGG was measured for the scaffold with 400 μm pores. The higher enhancement of Cu5 com-
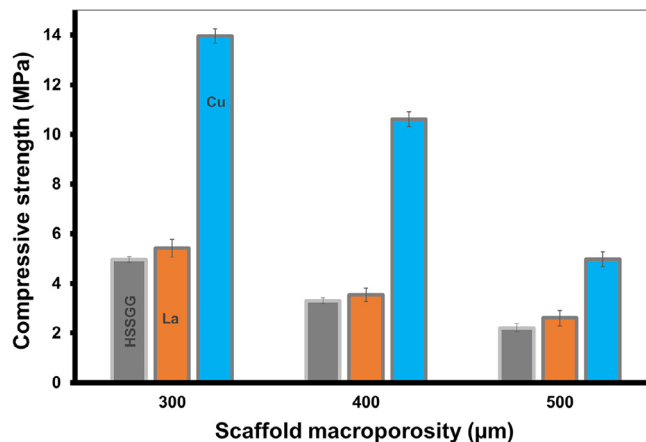

Fig. 7. Compressive strength of the scaffolds, fabricated from HSSGG, Cu5 and La5 glasses, with different macro–pore sizes (300, 400 and 500 μm) sintered at 800 °C.

pared to La5 can be attributed to the differences in ionic radii. The much smaller ionic radius of Cu (0.73 Å), in comparison to that of La (1.06 Å), [42], and its lower valence, confer to Cu a higher thermal diffusivity upon sintering the scaffolds. This enables Cu to act as an effective sintering aid, enhancing densification and the mechanical properties, as reported in Table 2 and Fig. 6. This fluxing role of Cu has been already explored to prepare mullite whiskers from kaolinite [45]. Therefore, doping the parent HSSGG glass with Cu exerts a remarkable improvement in the mechanical properties. It is suggested that doping HSSGG is a good option towards tailoring the mechanical properties for specific applications. Considering that individual La and Cu doping led to slight and accentuated increases in the compressive strength, their combined effects in different quantities are likely to be explored in future studies aiming at widening the range of potential applications for the implants. When the Archimedes method was used to determine the apparent porosity of the sintered scaffolds

Table 2
The corresponding compressive strength for sintered scaffolds with 300, 400 and 500 μm macropores for HSSGG, La5 and Cu5 glasses.

Macropores (μm)	Compressive strength (MPa)		
	HSSGG	La5	Cu5
300	4.9 ± 0.12	5.4 ± 0.34	13.9 ± 0.28
400	3.3 ± 0.11	3.5 ± 0.26	10.6 ± 0.29
500	2.2 ± 0.29	2.6 ± 0.30	4.9 ± 0.29

(300 μm), the average values of six measurements were 46.7% ± 1.8% for HSSGG, 42.6% ± 1.2% for La5, and 37.8% ± 1.5% for Cu5.

The statistical analysis using ANOVA showed F >> Fcrit, and P << 0.05, which led us to reject the null hypothesis and to confirm that significant improvement in the mechanical improporties can be achieved by doping HSSGG with La5 and Cu5. Furthermore, the decrease in the macropores from 500 to 300 μm led to a significant increase in the mechanical properties.

The statistical analysis confirms an interaction between the macropore size (300, 400 or 500 μm) as one factor, and the glass type (HSSGG, La5 or Cu5) as another factor, i.e. the interaction tells us that the effect of porosity on the compressive strength is dependent on the glass type, and also that the effect of the glass type on the compressive strength is dependent on the macroporosity.

3.5. Influences of ion doping on morphological surface features of scaffolds

Fig. 8 displays the SEM micrographs of HSSGG, (a, b), Cu5 (c, d) and La5 (e, f). The observation of these samples enables us to conclude that the parent HSSGG composition is the less prone to densification, with a higher intrinsic porosity fraction left in the sintered microstructures, with large pores exhibiting non–uniform shapes. Moreover, the necks formed among the particles are less extensive for the HSSGG sample in comparison to the doped ones. The most extensive neck formation is observed for the Cu5 particles, which become strongly bonded together. This is consistent with the compressive strength values measured for Cu5 glass

scaffolds as discussed in the previous section. In the case of La5 glass, doping also enhanced the formation of necks among the particles upon sintering in comparison to parent glass, but in a less extensive manner in comparison to Cu5. These results suggest that doping ions are acting as sintering aids, favouring the bulk material diffusion process upon sintering. The differences between the two doping ions can be attributed to their different thermal diffusivities due to dissimilar ionic radii and valences [42]. The active fluxing agent role of Cu has been already demonstrated [45]. Moreover, CuO has a lower melting point 1325 °C [46] in comparison to La_2O_3 (2313 °C) [47], permitting earlier diffusion [45]. It is also likely that the morphologies of sintered microstructures somehow reflect the particle sizes, PSD and packing ability of the starting glass powders displayed in Fig. 1.

4. Conclusions

The aim of this research work was to disclose the effects of Cu^{2+} and La^{3+} ion doping on the printability of sol–gel derived glass pastes for robocasting, and on the mechanical properties of the resulting sintered scaffolds. The results revealed that doping tends to decrease the mean particle size of the milled powders, an effect that was more evident for La5 than for Cu5. The rheological properties of the 40 vol% solid loaded inks were also affected by doping the parent glass with 5 wt% of Cu or La. With doping, the pastes became gradually less stiff and the LVR was less extended in comparison to that of HSSGG, which exhibited the highest G'
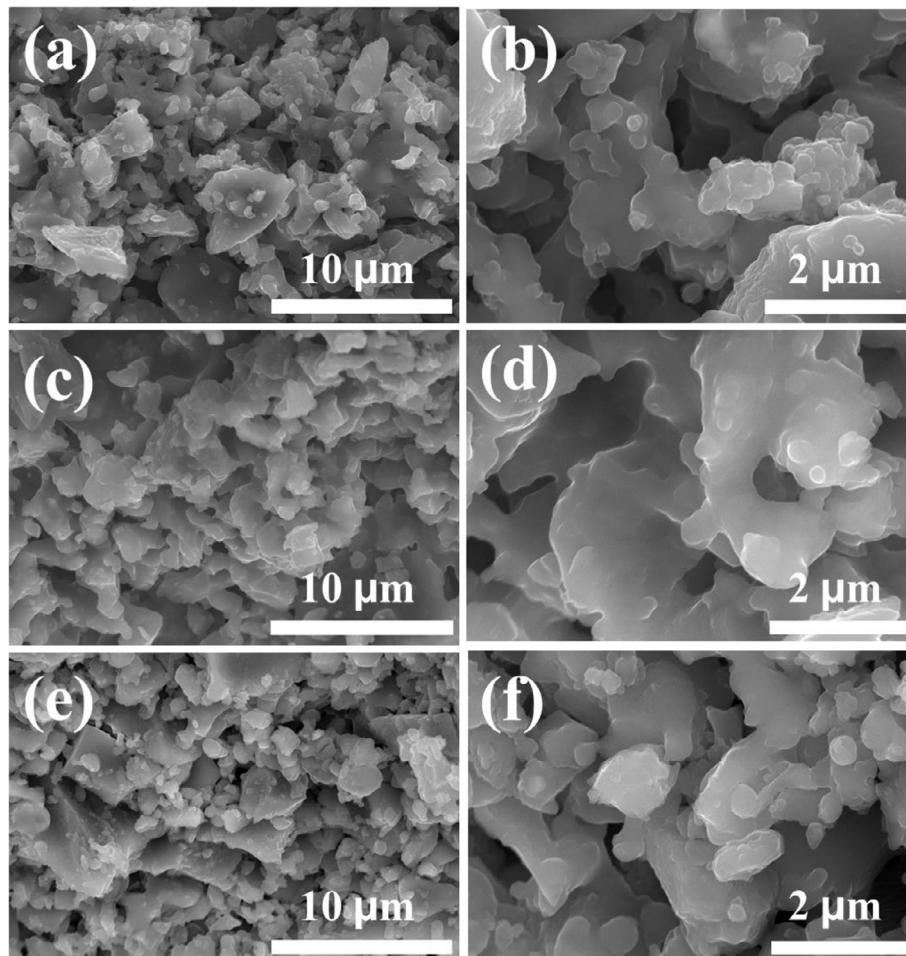

Fig. 8. Microstructural features of sintered scaffolds fabricated from the different glasses: (a, b) HSSGG; (c, d) Cu5; (e, f) La5.

of ~1 MPa, and the more extended LVR up to ~100 Pa. Nevertheless, the small differences in rheological properties affected neither the printability of all the pastes, nor the shape retention of the printed scaffolds. Although all scaffolds exhibited compressive strength values that fit well within the range reported for human cancellous bone (2–12 MPa), doping significantly enhanced their mechanical properties. This was particularly true in the case of Cu5, with increments up to 221% in comparison to those made of HSSGG. In the case of La5, only modest increments in compressive strength of 7%–18% were registered. These results confirm that glass doping is an important avenue to explore with the potential to greatly enhance the mechanical properties of scaffolds.

Acknowledgments

References

[1] I.D. Thompson, L.L. Hcnch, Mechanical properties of bioactive glasses, glass-ceramics and composites, Proc. Inst. Mech. Eng. Part H J. Eng. Med. 212 (1998) 127–136.

[2] M. Miola, A. Cochis, A. Kumar, C.R. Arciola, L. Rimondini, E. Verné, Copper-doped bioactive glass as filler for PMMA-based bone cements: morphological, mechanical, reactivity, and preliminary antibacterial characterization, Materials (Basel) 11 (2018).

[3] S. Kapoor, A. Goel, A. Tilocca, V. Dhuna, G. Bhatia, K. Dhuna, J.M.F. Ferreira, Role of glass structure in defining the chemical dissolution behavior, bioactivity and antioxidant properties of zinc and strontium co-doped alkali-free phosphosilicate glasses, Acta Biomater. 10 (2014) 3264–3278.

[4] M. Angelova, S. Asenova, V. Nedkova, Copper in the human organism, Trakia J. Sci. 9 (2011) 88–98.

[5] R. Uauy, M. Olivares, M. Gonzalez, Essentiality of Copper in Humans, Am. J. Clin. Nutr. 67 (1998) 9525–9598.

[6] V. Culotta, Cell Biology of copper, J. Biol. Inorg. Chem. 15 (2010) 1–2.

[7] J. Osredkar, N. Sustar, Copper and Zinc, Biological Role and Significance of Copper/Zinc Imbalance, J. Clin. Toxicol. s3 (2011) 1–18.

[8] H.H.A. Dollwet, J.R.J. Sorenson, Roles of copper in bone maintenance and healing, Biol. Trace Elem. Res. 18 (1988) 39–48.

[9] S. Soltani-Dehnavi, M. Mehdikhani-Nahrkhalaji, M. Rafienia, A. Doostmohammadi, Copper-doped and copper-free bioactive glass nanopowders cytotoxicity and antibacterial activity assessment, Sci. Iran. 24 (2017) 1706–1716.

[10] S. Zhao, L. Li, H. Wang, Y. Zhang, X. Cheng, N. Zhou, M.N. Rahaman, Z. Liu, W. Huang, C. Zhang, Wound dressings composed of copper-doped borate bioactive glass microfibers stimulate angiogenesis and heal full-thickness skin defects in a rodent model, Biomaterials 53 (2015) 379–391.

[11] L. Weng, S.K. Boda, M.J. Teusink, F.D. Shuler, X. Li, J. Xie, Binary Doping of Strontium and Copper Enhancing Osteogenesis and Angiogenesis of Bioactive Glass Nanofibers while Suppressing Osteoclast Activity, ACS Appl. Mater. Interfaces 9 (2017) 24484–24496.

[12] A. Bari, N. Bloise, S. Fiorilli, G. Novajra, M. Vallet-regí, G. Bruni, A. Torres-pardo, J.M. González-calbet, L. Visai, C. Vitale-brovarone, Copper-containing mesoporous bioactive glass nanoparticles as multifunctional agent for bone regeneration, Acta Biomater. 55 (2017) 493–504.

[13] A. Hoppe, R. Meszaros, C. Stähli, S. Romeis, J. Schmidt, W. Peukert, B. Marelli, S. N. Nazhat, L. Wondraczek, J. Lao, E. Jallot, A.R. Boccaccini, In vitro reactivity of Cu doped 45S5 Bioglass?? derived scaffolds for bone tissue engineering, J. Mater. Chem. B. 1 (2013) 5659–5674.

[14] L.B. Romero-Sánchez, M. Marí-Beffa, P. Carrillo, M.Á. Medina, A. Díaz-Cuenca, Copper-containing mesoporous bioactive glass promotes angiogenesis in an in vivo zebrafish model, Acta Biomater. 68 (2018) 272–285, https://doi.org/10.1016/j.actbio.2017.12.032.

[15] C. Wu, Y. Zhou, M. Xu, P. Han, L. Chen, J. Chang, Y. Xiao, Copper-containing mesoporous bioactive glass scaffolds with multifunctional properties of angiogenesis capacity, osteostimulation and antibacterial activity, Biomaterials 34 (2013) 422–433, https://doi.org/10.1016/j.biomaterials.2012.09.066.

[16] D.M. Taylor, R.W. Leggett, A generic biokinetic model for predicting the behaviour of the lanthanide elements in the human body, Radiat. Prot. Dosimetry. 105 (2003) 193–198.

[17] F. Bronner, Metals in Bone. Aluminum, Boron, Cadmium, Chromium, Lanthanum, Lead, Silicon, and Strontium., in: Princ. Bone Biol, 3rd editio,., Academic Press Inc, Farmington, 2008, pp. 515–531.

[18] T. Das, A. Sharma, G. Talukder, Effects of lanthanum in cellular systems - a review, Biol. Trace Elem. Res. 18 (1988) 201–228.

[19] D.M. Kramsch, A.J. Aspen, C.S. Apstein, Suppression of experimental atherosclerosis by the Ca++-antagonist lanthanum. Possible role of calcium in atherogenesis, J. Clin. Invest. 65 (1980) 967–981.

[20] D.M. Weekes, Lanthanum Complexes As Therapeutic Agents for the Treatment of bone resorption, disorders (2016).

[21] M. Ershad, V.K. Vyas, S. Prasad, A. Ali, R. Pyare, Synthesis and characterization of cerium- and lanthanum containing bioactive glass, Key Eng. Mater. 751 (2017) 617–628.

[22] X. Wang, L. Yuan, J. Huang, T.L. Zhang, K. Wang, Lanthanum enhances in vitro osteoblast differentiation via pertussis toxin-sensitive Gi protein and ERK signaling pathway, J. Cell. Biochem. 105 (2008) 1307–1315.

[23] J.E. Ellingsen, E.M. Pinholt, Pretreatment of titanium implants with lanthanum ions alters the bone reaction, J. Mater. Sci. Mater. Med. 6 (1995) 125–129.

[24] C.R. Gautam, S. Kumar, V.K. Mishra, S. Biradar, Synthesis, structural and 3-D architecture of lanthanum oxide added hydroxyapatite composites for bone implant applications: enhanced microstructural and mechanical properties, Ceram. Int. 43 (2017) 14114–14121.

[25] B.A.E. Ben-Arfa, I.M.M. Salvado, J.M.F. Ferreira, R.C. Pullar, Enhanced bioactivity of a rapidly-dried sol-gel derived quaternary bioglass, Mater. Sci. Eng. C. 91 (2018) 36–43.

[26] B.A.E. Ben-Arfa, A.S. Neto, I.E. Palamá, I.M. Miranda Salvado, R.C. Pullar, J.M.F. Ferreira, Robocasting of ceramic glass scaffolds: Sol–gel glass, new horizons, online as corrected proof, J. Eur. Ceram. Soc. (2018).

[27] B.A.E. Ben-Arfa, I.E. Palamá, M.F.F. José, Isabel M. Miranda, R.C.P.A. Salvado, Cytotoxicity and bioactivity assessments for Cu2+ and La3+ doped high silica sol–gel derived glasses (submited)(ID-MSEC-2018-2814), Mater. Sci. Eng. C. (2018).

[28] B.A.E. Ben-Arfa, A.S. Neto, I.M.M. Salvado, R.C. Pullar, José M.F. Ferreira, Robocasting: prediction of ink printability in sol-gel bioactive glass (accepted), J Am Chem Soc. (2018).

[29] F.J. O'Brien, Biomaterials & scaffolds for tissue engineering, Mater. Today. 14 (2011) 88–95.

[30] I. Bružauskaitė, D. Bironaitė, E. Bagdonas, E. Bernotienė, Scaffolds and cells for tissue regeneration: different scaffold pore sizes—different cell effects, Cytotechnology 68 (2016) 355–369.

[31] V. Karageorgiou, D. Kaplan, Porosity of 3D biomaterial scaffolds and osteogenesis, Biomaterials 26 (2005) 5474–5491, https://doi.org/10.1016/j.biomaterials.2005.02.002.

[32] S.F. Hulbert, F.A. Young, R.S. Mathews, J.J. Klawitter, C.D. Talbert, F.H. Stelling, Potential of Ceramic Materials as Permanently Implantable Percutaneous Devices, J. Biomed. Mater. Res. 4 (1970) 433–456.

[33] A. Ashman, M.L. Moss, Implantation of porous polymethylmethacrylate resin for tooth and bone replacement, J. Prosthet. Dent. 37 (1977) 657–665.

[34] T. Hausner, R. Schmidhammer, S. Zandieh, R. Hopf, A. Schultz, S. Gogolewski, H. Hertz, H. Redl, Nerve regeneration using tubular scaffolds from biodegradable polyurethane, Acta Neurochir. Suppl. 100 (2007) 69–72.

[35] M. Houmard, Q. Fu, E. Saiz, A.P. Tomsia, Sol–gel method to fabricate CaP scaffolds by robocasting for tissue engineering, J. Mater. Sci. Mater. Med. 23 (2012) 921–930.

[36] J.M. Karp, P.D. Dalton, M.S. Shoichet, Scaffolds for Tissue Engineering, MRS Bull. 301–306 (2003).

[37] E. Feilden, E.G.T. Blanca, F. Giuliani, E. Saiz, L. Vandeperre, Robocasting of structural ceramic parts with hydrogel inks, J. Eur. Ceram. Soc. 36 (2016) 2525–2533.

[38] S. Eqtesadi, A. Motealleh, P. Miranda, A. Pajares, A. Lemos, J.M.F. Ferreira, Robocasting of 45S5 bioactive glass scaffolds for bone tissue engineering, J. Eur. Ceram. Soc. 34 (2014) 107–118.

[39] S.M. Olhero, H.R. Fernandes, C.F. Marques, B.C.G. Silva, J.M.F. Ferreira, Additive manufacturing of 3D porous alkali-free bioactive glass scaffolds for healthcare applications, J. Mater. Sci. 52 (2017) 12079–12088.

[40] B.A.E. Ben-Arfa, H.R. Fernandes, I.M. Miranda Salvado, J.M.F. Ferreira, R.C. Pullar, Synthesis and bioactivity assessment of high silica content quaternary glasses with Ca: P ratios of 1.5 and 1.67, made by a rapid sol-gel process, J. Biomed. Mater. Res. - Part A. 106 (2018) 510–520.

[41] S. Eqtesadi, A. Motealleh, P. Miranda, A. Lemos, A. Rebelo, J.M.F.F. Ferreira, A simple recipe for direct writing complex 45S5 Bioglass®3D scaffolds, Mater. Lett. 93 (2013) 68–71.

[42] A.F. Wells, Structural Inorganic Chemistry, 4th ed., Oxford University Press, London, 1975.

[43] N. Gaddama, H.R. Fernandes, D.U. Tulyaganov, J.M.F. Ferreira, The structural role of lanthanum oxide in silicate glasses (submitted). Manuscript number: NOC-D-18-01218. (2018).

[44] D.R. Carter, G.H. Schwab, D.M. Spengler, Tensile Fracture of Cancellous Bone, Acta Orthop. Scand. 51 (1980) 733–741.

[45] S. Agathopoulos, H.R. Fernandes, D. Tulyaganov, J.M.F. Ferreira, Preparation of mullite whiskers from kaolinite using CuSO4 as fluxing agent, Mater. Sci. Forum. 455–456 (2004) 818–821.

[46] H.S. Roberts, H. Smyth, System copper: cupric oxide: oxygen, J. Am. Chem. Soc. 43 (1921) 1061–1079.

[47] O. Polyakov, Technology of Ferroalloys with Rare-Earth Metals, in: Handb. Ferroalloys, Twelfth Ed, Elsevier Ltd, 2013, pp. 459–469.